

MAPD-Net: A GPR-Based Method for Estimating Rebar Parameters and Concrete Moisture Content

Hai-Han Sun, *Member, IEEE*

Abstract—Ground-penetrating radar (GPR) is an efficient non-destructive technique for inspecting reinforced concrete structures. Estimating reinforcing bar (rebar) parameters from GPR radargrams remains challenging due to the strong correlation among rebar-related parameters when producing the reflection signature. Additionally, the unknown rebar orientation affects GPR detection capabilities and adds further difficulties in rebar parameter estimation, which has not yet been addressed in the existing literature. To tackle these issues, we present a neural network structure, called Multi-Polarimetric Aggregation and Parameter Decorrelation Neural Network (MAPD-Net), to automatically derive multiple rebar and concrete parameters from GPR radargrams. These parameters include concrete moisture content (mc), rebar cover depth (d), radius (r), and orientation (φ). Given multi-polarization radargrams as inputs, the MAPD-Net extracts informative features from each polarization radargram, weakens parameter correlation, and performs estimation of each parameter. Numerical results demonstrate that the MAPD-Net achieves high estimation accuracy in estimating these parameters. The mean absolute errors of mc , d , r , and φ in the 600 testing data are 0.06%, 0.8 mm, 0.4 mm, and 1.0°, respectively. The average absolute percentage errors of them are 2.2%, 1.1%, 3.8%, 4.4%, respectively.

Index Terms—Ground-penetrating radar, multi-polarization, neural network, parameter decorrelation, parameter estimation.

I. INTRODUCTION

GROUND-PENETRATING radar (GPR) has been widely used in the inspection of reinforced concrete structures. Locating reinforcing bars (rebars) and estimating their radius, orientation, and surrounding concrete properties are critical for structural health evaluation. However, the rebar reflection in a radargram results from the combined effect of multiple parameters. It is challenging to isolate the effect of a single parameter on the reflection signature because changes in one parameter may lead to changes in the reflection that are similar to those caused by another parameter. Therefore, the correlation among multiple rebar and concrete parameters when producing the rebar reflection signature makes the parameter estimation an ill-posed problem [1].

Several conventional methods have been investigated to derive the cover depth and radius of a rebar and/or its surrounding concrete properties. As the geometry of the rebar's hyperbolic reflection signature contains information on dominant rebar parameters, pattern-based methods were developed to derive rebar parameters from the hyperbolic arc [2]–[6]. Based on the influence of the rebar radius on the

Manuscript received May 03, 2024, revised June 24, 2024. This work was supported by the University of Wisconsin-Madison start-up package. (Corresponding author: Hai-Han Sun)

Hai-Han Sun is with the Department of Electrical and Computer Engineering, University of Wisconsin-Madison, Madison, WI 53706 USA (e-mail: haihan.sun@wisc.edu).

radar cross section for orthogonal polarizations, the radius can be extracted from the ratio of the backscattered energy of the rebar collected by orthogonal polarizations [7], [8]. Full-waveform inversion algorithms were presented in [9] to account for the radiation patterns of the electromagnetic source and receiver when characterizing rebar parameters. GPR antenna array combined with imaging methods were developed in [10] to produce high-resolution imaging of rebar and correlate it with rebar radius.

A common limitation of the aforementioned methods is that they are only valid when the rebar is orthogonally oriented to the GPR scanning trace and when the antenna polarization matches the rebar axis. However, this situation cannot be guaranteed due to deviations in orientation caused by construction errors or structural deficiencies. Different rebar orientations significantly affect the GPR detection capabilities of rebar, altering the shape and magnitude of the rebar reflection signature. This undermines the effectiveness of existing rebar parameter estimation methods and complicates GPR data interpretation [11].

Given the limitations of existing rebar characterization methods, advanced techniques are needed for accurate and simultaneous estimation of key rebar parameters. Since multiple rebar parameters collectively influence the rebar reflection signature in radargrams, a possible solution is to establish a non-linear mapping relationship between the features of the rebar reflection signature and multiple rebar parameters. Artificial intelligence algorithms, known for their robust feature extraction and learning capabilities, have demonstrated their effectiveness in rebar localization [16] and parameter estimation [17]. However, previous works have also neglected the cases of a rebar with different orientations, and the parameter estimation in [17] was performed based on A-scans collected on top of the rebar. Scenarios that deviate from this setup could result in estimation errors [17].

In this paper, to address the aforementioned limitations in both conventional and artificial intelligence algorithms, we present a Multi-Polarimetric Aggregation and Parameter Decorrelation Neural Network (MAPD-Net) that simultaneously estimates multiple rebar and concrete parameters based on multi-polarimetric radargrams. The parameters include the cover depth (d), radius (r), orientation (φ), and concrete moisture content (mc). The MAPD-Net takes the multi-polarimetric radargrams as inputs, extracts informative features of the rebar reflection signature via a Multi-Polarimetric Feature Extraction-Aggregation Module (MFEM), alleviates the adverse effects of parameter correlation and estimates four parameters in the Parameter Decorrelation-Estimation Module (PDM). Numerical experiments show that the MAPD-

Net achieves high accuracy in estimating these parameters. The novelty of this work is threefold. 1) To the best of our knowledge, this is the first work that considers the rebar orientation when estimating other rebar parameters, which enables a more robust and complete analysis of the rebar condition. 2) The MAPD-Net effectively addresses the adverse effects of parameter correlation, which greatly improves the estimation accuracy of each parameter. 3) The MAPD-Net successfully builds a non-linear mapping between multi-polarimetric radargrams and rebar and concrete parameters, enabling simultaneous and accurate parameter estimation. The accurately estimated parameters could facilitate subsurface rebar mapping and health examination of reinforced structures.

II. THE INFLUENCE OF DIFFERENT PARAMETERS ON MULTI-POLARIMETRIC RADARGRAMS

As a rebar depolarizes the incident waves based on its orientation, a multi-polarimetric GPR setup is adopted in this work for rebar detection. In this section, we briefly describe the influence of different rebar parameters and concrete moisture content on the radargrams collected by multi-polarimetric components (in short, multi-polarimetric radargrams). This GPR domain knowledge informs the neural network-based parameter estimation method as presented in Section III.

Fig. 1 shows the simulation scenario in gprMax [18] for numerical study. The concrete of different moisture content (mc) is modeled as a dispersive material with the Debye parameters provided in [17]. The rebar is modeled as a perfect electric conducting cylinder with a radius of r . It is located at a cover depth of d , and oriented at a horizontal angle φ . Orthogonally polarized (x - and y -polarized) sources and probes operating at a center frequency of 2 GHz are used as transmitters (TX) and receivers (RX) for rebar detection. They are spaced 100 mm apart and placed on the concrete surface. The scanning is performed by moving TX and RX along the x -direction with a step size of 25 mm. Reflected signals at 21 points along the scanning trace are collected by the multi-polarized TX/RX. Signals collected by each polarimetric component are combined into a two-dimensional B-scan radargram. Consequently, four multi-polarimetric radargrams, i.e., S_{xx} , S_{xy} , S_{yx} , and S_{yy} radargrams, are obtained in each scan, where the first and second subscripts in the polarimetric components denote the polarization of RX and TX, respectively.

The influence of each rebar and concrete parameter on the multi-polarimetric radargrams is studied by changing a single parameter value while setting others to default values. The default values are $mc = 6\%$, $d = 200$ mm, $r = 10$ mm, and $\varphi = 90^\circ$ unless otherwise specified.

Moisture content mc . Fig. 2(a) shows the multi-polarimetric radargrams with different mc . A higher mc results in a higher relative permittivity and conductivity of the concrete, leading to greater permittivity contrast between air and concrete, a lower propagation velocity of electromagnetic (EM) waves, and a larger attenuation of EM waves in the concrete. These factors produce stronger surface reflected signals, a later arrival time, a smaller amplitude, and a narrower hyperbolic curvature of the rebar reflection in the co-polarized

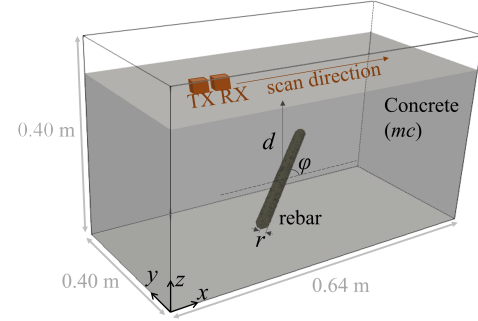


Fig. 1. Illustration of the simulation scenario of a rebar in concrete. Orthogonally polarized transmitter and receiver are used for rebar detection.

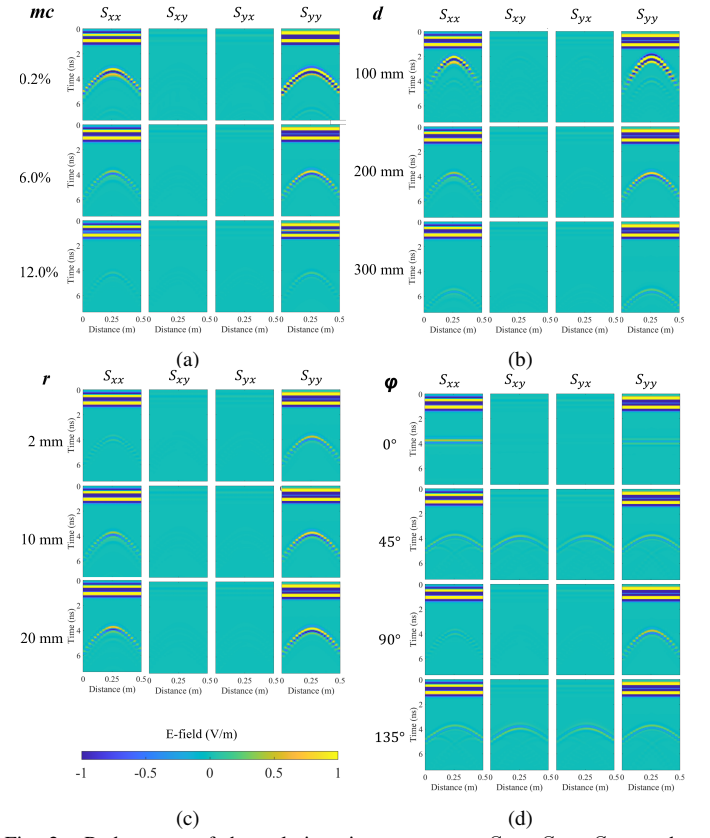


Fig. 2. Radargrams of the polarimetric components S_{xx} , S_{xy} , S_{yx} , and S_{yy} of a rebar with different (a) concrete moisture content mc , (b) depth d , (c) radius r , and (d) orientation angle φ . The parameters affect different characteristics of the radargrams, such as the spatial location, pixel value, and shape of rebar reflection signature. These characteristic features in multi-polarimetric radargrams can be used to estimate the rebar and concrete parameters.

S_{xx} and S_{yy} radargrams. Since the concrete has a flat surface that mainly reflects co-polarized signals, the surface reflection is not obvious in the cross-polarized S_{xy} and S_{yx} radargrams. Therefore, the information of mc is carried in the pixel value of the surface reflection, the pixel value, spatial position, and shape of the rebar reflection signature in the radargrams.

Depth d . Fig. 2(b) shows the multi-polarimetric radargrams with different d . A deeper location of a rebar leads to a later arrival time, a weaker strength of the rebar reflected signal, and a broader hyperbolic curvature. Therefore, the information of rebar depth is carried in the spatial location, pixel value, and shape of the rebar reflection signature in the radargrams.

Radius r . Fig. 2(c) shows the multi-polarimetric radargrams with different r . A rebar with a larger radius produces a stronger signal strength and a broader hyperbolic curvature. When the rebar has a very small radius that is not comparable to the GPR wavelengths in concrete (λ at 2.0 GHz is around 50 mm in concrete with $mc = 6.0\%$), such as in the case of $r = 2$ mm, the rebar reflection is very weak in the S_{xx} radargram because the x -polarization is orthogonal to the rebar orientation, but S_{yy} can capture distinguishable object reflection thanks to polarization match. Therefore, the information of the rebar radius is carried in the pixel value and shape of the rebar reflection signature in the radargrams.

Orientation angle φ . Fig. 2(d) shows multi-polarimetric radargrams of a rebar with different φ . The rebar radius is set as 2 mm to better demonstrate the influence of φ . The orientation affects both the signal strength and the shape of the rebar reflection in radargrams. When $\varphi = 0^\circ$, S_{xx} collects the strongest rebar reflection as the rebar orientation is parallel to the x -direction. S_{xy} , S_{yx} , and S_{yy} collect little object reflection. In this case, the reflection shape appears as a horizontal line. As φ increases from 0° to 45° , the signal strength collected by S_{xx} decreases, whereas the strengths collected by S_{xy} , S_{yx} , and S_{yy} increase. As φ further increases from 45° to 90° , S_{yy} captures a larger strength of the reflected signal, whereas S_{xx} , S_{xy} , and S_{yx} collect smaller strengths. At 90° , S_{yy} reaches the maximum strength as the object orientation aligns with the y -direction. In addition, as φ increases from 0° to 90° , the reflection curve transitions from a flat pattern to a hyperbolic pattern. As φ further increases from 90° to 180° , the variations in signal strengths and reflection curves in the radargrams are opposite to those observed as φ increases from 0° to 90° . For φ in the range of $[90^\circ, 180^\circ]$, the rebar reflection pattern is identical with the case of $(180^\circ - \varphi)$ in the co-polarized S_{xx} and S_{yy} radargrams, as demonstrated in cases of $\varphi = 135^\circ$ and $\varphi = 45^\circ$. However, the signals in these two cases are out of phase in the cross-polarized S_{xy} and S_{yx} radargrams. This information is the key to differentiating between these cases. Therefore, the information of $\varphi = 135^\circ$ is carried in the differences in the pixel value and shape of the rebar reflection signature in different polarimetric radargrams.

In summary, the rebar reflection signature in multi-polarimetric radargrams results from the combined effects of multiple parameters. As mc impacts most of the radargram features, it is the easiest parameter to estimate, followed by d , with r and φ being the most challenging. This hierarchy allows us to use the more-information-related parameters as priors to enhance the estimation of less-information-related parameters, thereby reducing estimation uncertainties due to parameter correlation. Therefore, in this work, we aim to build a deep neural network model to map the relationship between the characteristics of multi-polarimetric radargrams and rebar and concrete parameters while alleviating parameter correlation to improve the accuracy of parameter estimation.

III. METHODOLOGY

In this section, we present a novel network structure, the MAPD-Net, to estimate multiple rebar parameters and

concrete moisture content. The MAPD-Net is composed of the Multi-Polarimetric Feature Extraction-Aggregation Module (MFEM) and Parameter Decorrelation-Estimation Module (PDM), as shown in Fig. 3.

MFEM. Since different polarimetric radargrams (i.e., S_{xx} , S_{xy} , S_{yx} , S_{yy}) carry complementary information of rebar parameters as discussed in Section II, the MFEM is designed to extract and aggregate the informative and complementary features of each polarimetric radargram. The MFEM consists of four paths to extract independent features from each polarimetric radargram and one path to extract complementary features from concatenated radargrams. In each path, the radargram is first forwarded to a residual block [22] to obtain coarse features, followed by three consecutive operations of a convolutional layer and a feature aggregation (FA) block, along with two downsampling operations to refine the features. Since a rebar with different parameters produces reflection signature in different spatial regions in the radargram, an FA block is designed to expand the receptive fields of the MFEM and extract the multi-scale rebar reflection information.

The FA block adopts a three-branch feature extraction mechanism, as shown in Fig. 4. In each branch, the input feature maps are first passed through an average pooling layer with different downsampling rates to obtain features in different scales. They are then forwarded to a convolutional layer followed by an upsampling operation to the original dimensions. The upsampled feature maps from different sub-branches are added up and then passed through another convolutional layer to obtain the final output feature maps. Since a larger downsampling rate corresponds to a larger receptive view, fusing the features of three different scales allows the FA block to achieve a multi-scale receptive field. We would like to note that the "downsample-convolution-upsampling" operation in the FA block can be replaced with the dilated convolutions without compromising network performance.

Next, the extracted features from the five paths are concatenated and forwarded to two residual blocks. The residual blocks not only aggregate the polarimetric dependent features, but also reduce the number of feature maps to alleviate the computational burden. The output of the second residual block is passed to the PDM for the estimation of multiple parameters.

PDM. The PDM is designed as a four-branch module to simultaneously estimate the four parameters. As the output of MFEM contains abundant features, and different parameters have tighter connections with some features than others, it is feasible to first highlight the informative features related to the corresponding parameter, and then pass them to a fully connected layer for parameter estimation. To this end, we employ a channel attention (CA) block [20] in each branch to emphasize informative features and suppress less useful ones. After the CA module, the recalibrated features are processed through a convolutional layer and then fed to two consecutive fully-connected layers to estimate the corresponding parameter. As discussed in Section II, the influences of the four rebar and concrete parameters on the radargrams are tightly correlated, but some parameters, such as mc and d , correspond to more information in radargrams, while others, such as r and φ , are related to less information. Therefore, the

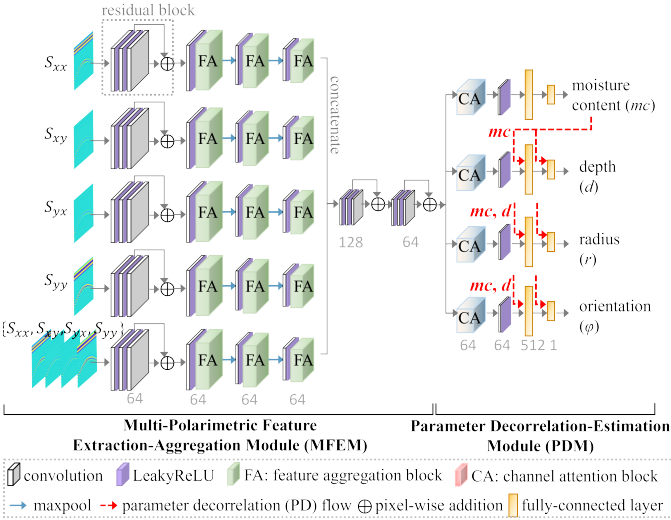


Fig. 3. The framework of the MAPD-Net. It is composed of a Multi-Polarimetric Feature Extraction-Aggregation Module (MFEM) to extract and integrate informative features related to parameter estimation from the four polarimetric radargrams, and a Parameter Decorrelation-Estimation Module (PDM) to simultaneously estimate multiple rebar and concrete parameters. The numbers shown in the figure indicate the numbers of output feature channels or nodes.

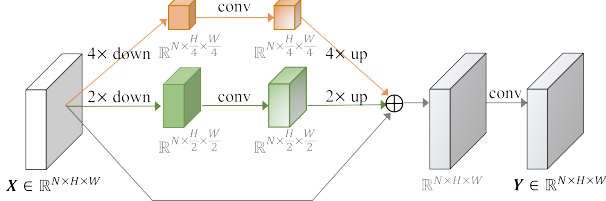


Fig. 4. Illustration of the feature aggregation (FA) block. It comprises three subbranches, each of which extracts features in different scales. The features in all sub-branches are upsampled to the original dimensions and then combined as the final output. The FA block effectively expands the receptive view of the MFEM.

estimation difficulty and accuracy of these parameters differ significantly. To tackle this issue, we specifically introduce parameter decorrelation (PD) flows to feed the more-information-related parameters as priors to the estimation branches of less-information-related parameters, as indicated by the red dotted lines in Fig. 3. By doing so, the influence of more-information-related parameters can be decoupled from the features associated with less-information-related parameters, thereby enhancing the estimation accuracy.

Loss Function. A multi-task loss function is used to drive the optimization of the network, which is expressed as

$$L = L_{mc} + L_d + L_r + L_\varphi, \quad (1)$$

where L_{mc} , L_d , L_r , and L_φ are the mean squared error between the estimated value and the corresponding ground truth of mc , d , r , and φ , respectively.

IV. EXPERIMENTS

A. Implementation Details of the MAPD-Net

To implement the MAPD-Net, we generate 3000 sets of data for a rebar with different parameters using gprMax [18]. Each set of data includes the radargrams of S_{xx} , S_{xy} , S_{yx} , S_{yy} , and the corresponding ground truth of mc , d , r , and φ . The scenario is the same as the one shown in Fig. 1. Following the

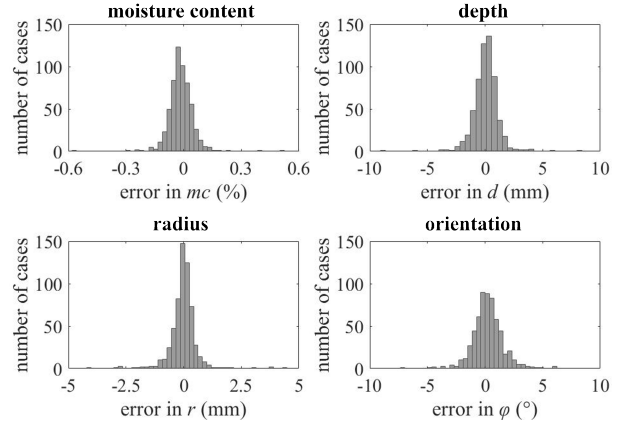


Fig. 5. The histograms of estimation errors in rebar and concrete parameters.

parameter settings in [17], the moisture content of the concrete is within the range of 0.2% to 12.0%, and the rebar cover depth, radius, and orientation angle are within the range of 0 to 300 mm, 2 mm to 25 mm, and 0 to 179°, respectively. In each case, the rebar and concrete parameters are randomly selected within their corresponding ranges. Other setups are the same as those provided in Section II.

The 3000 sets of data are randomly divided into training (80%) and testing (20%) sets. The radargrams are resized to 128×24 and scaled to the range of [0, 1] based on the maximum and minimum values of all the radargrams of different polarizations. The MAPD-Net is implemented using PyTorch on an NVIDIA RTX 4090 GPU. The weights are initialized with the standard Gaussian function. The batch size is set as 20. The optimization of the network is performed using the ADAM optimizer [21] with default parameters. The initial learning rate is set as 0.0001 and decreases by a factor of 10 every 40 epochs. The model is trained for 200 epochs from scratch.

B. Experimental Results of the Estimation Accuracy

The well-trained MAPD-Net is applied to estimate the rebar and concrete parameters of the 600 testing data. The histograms of estimation errors of mc , d , r , and φ are shown in Fig. 5. 99% of data having an estimation error within $\pm 0.3\%$ for mc , within ± 5 mm for d , within ± 2.5 mm for r , and within $\pm 5^\circ$ for φ . The mean absolute errors (MAEs) of mc , d , r , and φ in the 600 testing data are 0.06%, 0.8 mm, 0.4 mm, and 1.0°, respectively. Considering their different ranges, their mean absolute percentage errors (MAPEs) are also calculated, which are 2.2%, 1.1%, 3.8%, 4.4%, respectively. The low MAEs and MAPEs on the testing data prove the network's capability in accurately estimating multiple rebar and concrete parameters.

C. Ablation Study

Ablation study is conducted to demonstrate the effectiveness of the key components of the MAPD-Net on the parameter estimation accuracy. These components include the branches of S_{xy} and S_{yx} radargrams, the fifth branch of the cascaded multi-polarimetric radargrams, the FA block, the CA block, and the PD flow. The mean absolute percentage errors

TABLE I
COMPARISON OF PARAMETER ESTIMATION ACCURACY IN ABLATION STUDY (THE BEST RESULTS ARE HIGHLIGHTED IN BLUE.)

Networks	A	B	C	D	E	MAPD-Net
S_{xy} and S_{yx} radargrams		✓	✓	✓	✓	✓
the fifth branch of the cascaded radargrams	✓		✓	✓	✓	✓
FA blocks	✓	✓		✓	✓	✓
CA blocks	✓	✓	✓		✓	✓
PD flows	✓	✓	✓	✓		✓
MAPE (mc)	2.3%	2.2%	3.5%	2.3%	2.2%	2.2%
MAPE (d)	1.3%	1.3%	2.0%	1.5%	1.6%	1.1%
MAPE (r)	6.0%	6.3%	6.1%	6.6%	7.2%	3.8%
MAPE (φ)	72.0%	5.9%	6.0%	6.4%	6.2%	4.4%

(MAPEs) of the ablation networks are presented in Table I. Compared to the ablated networks, it is clear that the final MAPD-Net achieves the highest estimation accuracy for each parameter. The ablation study validates that by using multi-polarimetric radargrams as inputs, implementing FA blocks to extract features from different receptive fields, using CA blocks to emphasize informative features related to each parameter, and employing the PD mechanism to decouple the parameters in the final estimation stage, the network effectively establishes the relationship between the multi-polarimetric radargrams and the rebar and concrete parameters, and therefore achieves the highest estimation accuracy.

V. CONCLUSION

In this paper, we present a neural network structure, the MAPD-Net, for estimating multiple rebar parameters and concrete moisture content based on multi-polarimetric radargrams. MAPD-Net is specially designed with two modules to extract informative features from multi-polarized radargrams and establish their relationship with rebar and concrete parameters, thereby enabling accurate parameter estimation. The introduction of PD flows within the network mitigates the adverse effects of parameter correlation on estimation accuracy. Numerical experiments verify that the MAPD-Net estimates the four rebar parameters of interest with high accuracy. This is the first work that takes into account the rebar orientation while estimating other rebar parameters. The automatic and accurate estimation of multiple rebar parameters and concrete moisture content could facilitate the examination of structural integrity and quality control of reinforced concrete buildings. Future work will focus on extending the network's effectiveness to measured rebar data in the field, and using the method to monitor parameter changes in the corrosion process. These efforts will potentially expand the network's applicability to corrosion damage evaluation and structural health examination.

REFERENCES

- [1] I. Giannakis, F. Zhou, C. Warren, and A. Giannopoulos, "On the limitations of hyperbola fitting for estimating the radius of cylindrical targets in nondestructive testing and utility detection," *IEEE Geosci. Remote Sens. Lett.*, vol. 19, pp. 1-5, 2022.
- [2] L. Borgioli, P. Capineri, S. Falorni, Matucci, C. G. Windsor, "The detection of buried pipes from time-of-flight radar data," *IEEE Trans. Geosci. Remote Sens.*, vol. 46, no. 8, pp. 2254-2266, Aug. 2008.
- [3] A. V. Ristic, D. Petrovacki, and M. Govedarica, "A new method to simultaneously estimate the radius of a cylindrical object and the wave propagation velocity from GPR data," *Comput. Geosci.*, vol. 35, no. 8, pp. 1620-1630, Aug. 2009.
- [4] S. Shihab and W. Al-Nuaimy, "Radius estimation for cylindrical objects detected by ground penetrating radar," *Subsurf. Sens. Technol. Appl.*, vol. 6, no. 2, pp. 151-166, Jul. 2005.
- [5] W. Al-Nuaimy, Y. Huang, A. Eriksen and V. T. Nguyen, "Automatic detection of hyperbolic signatures in ground-penetrating radar data," *Proc. SPIE*, vol. 4491, pp. 327-335, Nov. 2001.
- [6] C. Windsor, L. Capineri, P. Falorni, S. Matucci, and G. Borgioli, "The estimation of buried pipe diameters using ground penetrating radar," *Insight: Non-Destr. Test. Cond. Monit.*, vol. 47, no. 7, pp. 394-399, Jul. 2005.
- [7] L. Zanzi and D. Arosio, "Sensitivity and accuracy in rebar diameter measurements from dual-polarized GPR data," *Constr. Build. Mater.*, vol. 48, pp. 1293-1301, Nov. 2013.
- [8] H. H. Sun, W. Cheng, and Z. Fan, "Diameter estimation of cylindrical metal bar using wideband dual-polarized ground-penetrating radar," *IEEE Trans. Instrum. Meas.*, vol. 72, pp. 1-14, 2023.
- [9] I. Giannakis, A. Giannopoulos, and C. Warren, "A Machine Learning Scheme for Estimating the Diameter of Reinforcing Bars Using Ground Penetrating Radar," *IEEE Geosci. Remote Sens. Lett.*, vol. 18, no. 3, pp. 461-465, Mar. 2021.
- [10] W. Cheng, H. H. Sun, K. H. Tan, and Z. Fan, "Estimating the diameter of reinforcing bars using an ultra-wideband MIMO GPR array," *Constr. Build. Mater.*, vol. 365, pp. 129924, Feb. 2023.
- [11] Z. Xiang, G. Ou, and A. Rashidi, "Integrated approach to simultaneously determine 3D location and size of rebar in GPR data," *J. Perform. Constr. Facil.*, vol. 365, pp. 129924, Feb. 2023.
- [12] M. Lualdi and F. Lombardi, "Significance of GPR polarisation for improving target detection and characterisation," *Nondestruct. Test. Evaluation*, vol. 29, no. 4, pp. 345-356, Aug. 2014.
- [13] H. Liu, J. Zhao, and M. Sato, "A hybrid dual-polarization GPR system for detection of linear objects," *IEEE Antennas Wireless Propag. Lett.*, vol. 14, pp. 317-320, 2015.
- [14] A. Villela and J. M. Romo, "Invariant properties and rotation transformations of the GPR scattering matrix," *J. Appl. Geophys.*, vol. 90, pp. 71-81, 2013.
- [15] H. Liu, X. Huang, F. Han, J. Cui, B. F. Spencer, and X. Xie, "Hybrid polarimetric GPR calibration and elongated object orientation estimation," *IEEE J. Sel. Topics Appl. Earth Observ. Remote Sens.*, vol. 12, no. 7, pp. 2080-2087, Jul. 2019.
- [16] H. Liu, C. Lin, J. Cui, L. Fan, X. Xie, and B. F. Spencer, "Detection and localization of rebar in concrete by deep learning using ground penetrating radar," *Autom. Constr.*, vol. 118, pp. 103279, Oct. 2020.
- [17] I. Giannakis, A. Giannopoulos and C. Warren, "A machine learning scheme for estimating the diameter of reinforcing bars using ground penetrating radar," *IEEE Geosci. Remote Sens. Lett.*, vol. 18, pp. 461-465, Mar. 2021.
- [18] C. Warren A. Giannopoulos and I. Giannakis, "gprMax: Open source software to simulate electromagnetic wave propagation for Ground Penetrating Radar," *Comput. Phys. Commun.*, vol. 209, pp. 163-170, 2016.
- [19] K. He, X. Zhang, S. Ren, and J. Sun, "Deep residual learning for image recognition," in *IEEE CVPR*, Las Vegas, NV., USA, 2016, pp. 770-778.
- [20] J. Hu, L. Shen, and G. Sun, "Squeeze-and-excitation networks," in *IEEE CVPR*, Salt Lake City, UT, USA, 2018, pp. 7132-7141.
- [21] D. P. Kingma and J. Ba, "Adam: A method for stochastic optimization," in *Proc. ICLR*, San Diego, CA, USA, 2015, pp. 1-18.